Proceedings of 29th International Conference on Ocean, Offshore and Arctic Engineering
OMAE 2010
June 6-11, 2010, Shanghai, China

OMAE2010-20030

INTERMEDIATE OCEAN WAVE TERMINATION USING A CYCLOIDAL WAVE ENERGY CONVERTER

Stefan G. Siegel*

Department of Aeronautics
United States Air Force Academy
Air Force Academy, Colorado, 80840
USA
Email: stefan@siegels.us

Tiger Jeans

Department of Aeronautics
United States Air Force Academy
Air Force Academy, Colorado, 80840,
USA

Thomas McLaughlin

Department of Aeronautics
United States Air Force Academy
Air Force Academy, Colorado, 80840,
USA

ABSTRACT

We investigate a lift based wave energy converter (WEC), namely, a cycloidal turbine, as a wave termination device. A cycloidal turbine employs the same geometry as the well established Cycloidal or Voith-Schneider Propeller. The interaction of intermediate water waves with the Cycloidal WEC is presented in this paper. The cycloidal WEC consists of a shaft and one or more hydrofoils that are attached eccentrically to the main shaft and can be adjusted in pitch angle as the Cycloidal WEC rotates. The main shaft is aligned parallel to the wave crests and fully submerged at a fixed depth. We show that the geometry of the Cycloidal WEC is suitable for wave termination of straight crested waves. Two-dimensional potential flow simulations are presented where the hydrofoils are modeled as point vortices. The operation of the Cycloidal WEC both as a wave generator as well as a wave energy converter interacting with a linear Airy wave is demonstrated. The influence that the design parameters radius and submergence depth on the performance of the WEC have is shown. For optimal parameter choices, we demonstrate inviscid energy conversion efficiencies of up to 95% of the incoming wave energy to shaft energy. This is achieved by using feedback control to synchronize the rotational rate and phase of the Cycloidal WEC to the incoming wave. While we show complete termination of the incoming wave, the remainder of the energy is lost to harmonic waves travelling in the upwave and downwave direction.

NOMENCLATURE

T Wave Period [s]
D Water Depth [m]
H Wave Height [m]
C Wave Travel Velocity (Celerity) [m/s]
C_g Wave Group Velocity [m/s]
k Wave Number [1/m]
g Gravity constant, $9.81[m/s^2]$
t Time [s]
λ Wavelength [m]
R Wave Energy Converter Radius [m]
x_c, y_c Wave Energy Converter Shaft location [m]
Φ Flow Potential
η Water Surface
Γ Vortex or Hydrofoil Circulation $[m^2/s]$
$\delta(t)$ Main Shaft rotational angle $[deg]$
θ Feedback phase $[deg]$
$F(z,t) = \varphi + i\psi$ Complex Stream Function

INTRODUCTION

Among alternative energy sources, wave power is one of the most abundant sources on earth. The World Energy Council according to [1] has estimated the world wide annual amount of wave power energy at 17.5 PWh (Peta Watt hours = $10^{12} kWh$). This is actually comparable to annual world wide electric energy consumption, which is currently estimated at 16 PWh. Thus,

*Address all correspondence to this author.

wave power has the potential to provide a large portion of the worlds electric energy needs, if it can be tapped efficiently. In addition to the energy availability, wave power has other advantages. Since a large portion of the worlds population lives close to the ocean shores, the distance between energy production and consumption is small. This reduces transmission losses and necessary investments in transmission lines. As opposed to other alternative energy sources like wind, stream and solar energy, the installation of wave power devices does not require use of already precious real estate. This makes wave power an ideal energy source for efficiently providing renewable energy to densely populated coastal areas. Ocean waves have a tremendous potential to provide clean renewable energy. Further engineering aspects of wave power as an energy source are appealing as well. While the energy density of both solar and wind in typical favorable sites is in the order of $1kWm^{-2}$ according to [2], wave power at a typical US west coast location yields $25kWm^{-1}$ of wave crest (including all energy between the water surface and the ocean floor), potentially allowing much larger amounts of energy to be extracted with a converter of a given size. Furthermore, wave energy is available on a more consistent basis and can be better predicted in advance, therefore mitigating the need to back up a wave power plant with other conventional power sources, as is the case for both solar and wind energy.

MOTIVATION

Analysis of the different wave energy conversion devices that have been investigated or proposed reveals a number of commonalities in design. The first is that all devices require a connection to the sea bed in order to extract energy, which has two main drawbacks. First, a seabed connection makes the device vulnerable in rough seas and storms, in the same way as an anchored ship is vulnerable in a storm (and will likely break the anchor line). According to [1], storm survivability has been a major problem for many wave power devices, with some being destroyed by the elements as early as during deployment. Also, for most of the devices, the load imposed onto the seabed connection is proportional to the power which the device can extract. This means that the anchor point needs to be stronger and thus more costly as more energy is being extracted. Therefore, many of these devices cannot easily be scaled up to power plant levels of energy conversion. In addition, since the devices need to be anchored to the sea floor, they are not well suited to operation in deep water waves, where the ocean floor may be hundreds of meters away from the surface. However, most wave energy is contained in deep water waves, and the energy density of a wave decreases as it approaches shallow water. Thus, most devices cannot operate in the most promising locations for wave power extraction.

The second common design feature is that most wave power devices will only extract energy from one component of the wave

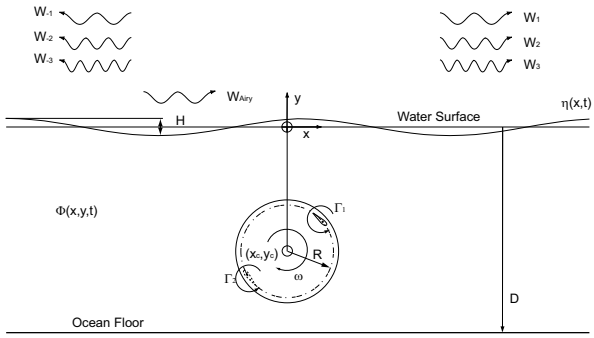

Figure 1. Cycloidal wave energy converter geometry

motion. For example, buoy devices will only extract energy from the vertical motion of the waves. However, in a shallow water wave, most kinetic energy is contained in flow oscillating in the horizontal direction, while in a deep water wave the kinetic energy is evenly split in horizontal and vertical oscillation. This limits a symmetric buoy in heave mode or oscillating water column device to a theoretically optimum energy extraction efficiency of 50%, according to [3]. If the device is small in the third dimension compared to the length of the incoming waves and thus constitutes a point absorber, the efficiency of the buoy or oscillating water column device drops further to a theoretical inviscid maximum of 25%. These reduced efficiencies are caused by radiation of waves from the wave energy converter that interfere destructively with the incoming wave. However, some buoy devices may achieve a capture width that is larger than the size of the buoy by operating in combined pitch and heave modes and / or using an asymmetric design.

In terms of wave far field, an optimal wave energy converter would create an out of phase wave with the same amplitude and wave length as the incoming wave, travelling in only one direction and exactly out of phase with the incoming wave. This wave energy converter, commonly referred to in literature as a wave termination device, could extract 100% of the energy of the incoming wave in the theoretical inviscid limit. Of all wave energy converters currently proposed or investigated in open literature, no design can achieve this. One main reason lies in the difficulty of preventing the wave energy converter from producing waves in the up–wave direction. Any wave travelling in the up–wave direction will reduce the efficiency of the converter, even in the inviscid limit. The same holds true for harmonic waves traveling in any direction.

A typical cycloidal wave energy converter as considered in this paper is shown in figure 1. It features one or more hydrofoils attached parallel to a main shaft at a radius R. While the shaft rotates, the orientation of the blades may be adjusted. Based on the sketch in figure 1, a number of non dimensional quantities emerge. The basic size of the wave energy converter will be denoted by $2R/\lambda$, where we use the wave length λ as the

fundamental length scale. Consequently, the depth of submergence is denoted by y_c/λ, and the wave height by H/λ. It is also convenient for parameter studies to compare different size wave energy converters while keeping the distance between the water surface and the topmost point of the cycloidal wave energy converter path fixed, that is $(y_c - R)/\lambda = const$. The direction of travel of an incoming ocean wave W_{Airy} is assumed to be left to right, and waves generated by the cycloidal wave energy converter that travel in the direction of the incoming wave receive a positive index and are considered traveling down–wave; while waves in the opposite direction are considered up–wave traveling and receive a negative index number. While the case of infinite water depth (deep water waves) has been investigated in detail by the same authors in [4], we investigate the impact of finite water depth D on the wave energy converter performance for intermediate water waves in this paper. Intermediate water waves are of interest since many locations closer to the ocean shore, including existing and proposed wave energy testing sites, feature intermediate water waves.

NUMERICAL METHOD

Simulation Setup

We present solutions to the velocity potential equation:

$$V = \nabla\varphi. \tag{1}$$

The solution is subject to a linearized free surface boundary condition as well as non-reflective radiation boundaries at the up–wave and down–wave ends of a two dimensional spatial domain. The complex potential for a vortex moving under a free surface with position $c(t) = a(t) + ib(t)$ in the complex plane is developed in [5] to be

$$\begin{aligned} F(z,t) = {} & \frac{\Gamma(t)}{2\pi i} ln(z - c(t)) - \frac{\Gamma(t)}{2\pi i} ln(z - \overline{c}(t) + 2iD) \\ & + \frac{\Gamma(t)}{\pi} \int_0^\infty \frac{e^{-kD}}{k\cosh(kD)} \\ & \times \sinh(b(t) + D)\sin(k(z - a(t) + iD))dk \\ & - \frac{g}{\pi} \int_0^\infty \frac{sech^2 kD}{\sqrt{gk\tanh(kD)}} dk \\ & \times \int_0^t \Gamma(\tau)\sinh(k(b(\tau) + D)\sin(k(z - a(\tau) + iD) \\ & \times \sin[\sqrt{gk\tanh(kD)}(t - \tau)]d\tau \end{aligned} \tag{2}$$

with $\Gamma(t)$ the circulation of the vortex, $g = 9.81ms^{-2}$ the gravity constant, and k the wave number. Equation 2 satisfies both the linearized kinematic and dynamic free surface boundary conditions at $y = 0$. The terms on the first line are the complex potential due to the vortex and its mirror image above the surface, which is necessary to satisfy the kinematic free surface condition. The remaining integrals describe the radiated waves related to the dynamic free surface condition.

For the simulations, the individual hydrofoils of the cycloidal wave energy converter are modeled as single vortices in the presence of a free surface using equation 2. Equation 2 is integrated using second order spatial and time marching techniques. A numerical resolution study has been performed in order to determine appropriate values of the wave number increment Δk,the maximum wave number considered k_{max} and the time discretization increment Δt, for details refer to [4]. Based on the investigations presented there for deep ocean waves it was concluded that the required resolutions for numerical convergence are $T/\Delta t = 36$, $k/\Delta k = 31.6$, and $k_{max}/k = 75.9$. Comparison of the intermediate ocean wave results presented here showed that these discretization time steps also deliver converged results for intermediate ocean waves. We also compared the results obtained with these integration parameters to a simulation using half the increment in time and wave number discretization and twice the maximum wave number. Both simulations predict nearly identical wave patterns, indicating that the chosen settings are sufficient, thus we use them in all simulations presented here.

$$\eta = -g\frac{\partial\varphi}{\partial t}, \tag{3}$$

Subsequent to solving the flow potential, equation 3 is used to determine the resulting wave pattern. This approach has been previously implemented by [6] for deep water waves, and comparison to our results show goods agreement.

Incoming Airy wave

In order to investigate the interaction of the cycloidal wave energy converter and an incoming wave, we resort to linear Airy wave theory. The velocity potential for a progressive linear intermediate depth wave is given in [7] to be

$$\varphi(x,y,t) = \frac{Hg}{\omega}\frac{\cosh(k(y + D))}{\cosh(kD)}\sin(kx - \omega t) \tag{4}$$

where H is the wave amplitude, D is the water depth, ω is the wave frequency and k is the wave number. Beyond the flow potential, Airy wave theory can be used to describe the wave traveling velocity or celerity C, group velocity C_g and wavelength λ_{Airy} based on the gravity constant $g = 9.81ms^{-2}$ and wave period T such that:

$$
\begin{aligned}
C &= \frac{g\,T_{Airy}}{2\pi}\tanh\left(\frac{2\pi D}{\lambda}\right)\\
C_g &= \frac{1}{2}\left[1+\frac{4\pi D/\lambda}{\sinh(4\pi D/\lambda)}\right]C\\
\lambda_{Airy} &= C\,T_{Airy}.
\end{aligned}
\tag{5}
$$

Typically, the wave energy converter will create more than a single plain traveling wave. The wave height of each generated wave component can be determined by Fourier analysis. Throughout this paper indices are used to identify the harmonic wave components and their traveling direction, as shown in figure 1. Waves traveling left or in the up–wave direction receive negative indices, while down–wave travelling waves receive positive indices. It is possible to determine the energy associated with each wave by employing Airy wave theory which relates wave power to wave height and period by:

$$
P = \frac{1}{8}\rho\, g\, H^2\, C_g \tag{6}
$$

Since the wave power scales linearly with the wave period T, higher harmonic waves of the same wave height will contain less energy in proportion to their period. Also to be noted is a quadratic relationship between wave energy and wave height H. Based on wave power, the figure of merit of the wave energy converter design becomes the ratio of the power in the (desired) fundamental wave traveling down–wave, P_1 which is used to cancel the incoming Airy wave, compared to the power contained in all waves:

$$
P_1/P_{all} = \frac{P_1}{\sum_{n=-\infty}^{\infty} P_n}. \tag{7}
$$

The power ratio will reach a value of one if only the desired down–wave traveling fundamental wave is created, and zero if no down–wave traveling fundamental wave is produced at all. The wave power analysis is based on energy conservation which is implicit in the unsteady Bernoulli equation, and on a control volume analysis assuming that all energy leaving or entering at the up–wave and down–wave boundaries is contained in traveling Airy type waves. Thus, the power difference at both boundaries is to be provided or absorbed by the traveling point vortex/vortices.

Wave Energy Converter motion The position of the vortex is prescribed as a function of time. The coordinates for the vortex moving about the center of rotation $(0, y_c)$ with radius R and frequency ω are

$$
\begin{aligned}
c_x(t) &= R\cos(\omega_c t+\theta),\\
c_y(t) &= y_c - R\sin(\omega_c t+\theta)
\end{aligned}
\tag{8}
$$

Thus, the motion of the converter starts with the first (or sole) blade being in the most down–wave position, and rotation is in the clockwise direction as shown in figure 1. An arbitrary phase shift θ is introduced, which indicates the relative phase between an incoming Airy wave and the cycloidal wave energy converter motion. The first or sole vortex is traveling up–wave for the first half rotation, and down–wave for the second half. Experiments conducted by [8] showed that the Cycloidal propeller is a naturally stable rotating system that automatically synchronizes itself to the rotational frequency of an incoming wave. While we do not rely on this self-synchronization capability in the present investigation, we limit ourselves to operation of the cycloidal propeller at the same rotational frequency ω_c as that of the incoming Airy wave:

$$
\omega_c = \omega_{Airy} \tag{9}
$$

Thus, the only independent variables in equation 8 are R, y_c, and for the wave cancellation simulations the wave amplitude H_{Airy} and phase difference θ in equation 8 between the incoming wave and the rotation of the cycloidal wave energy converter. The intermediate water depth is characterized by D/λ, where the parameter range $0.04 < D/\lambda < 0.5$ is considered an intermediate water wave. We show the impact of all of these parameters on the performance of the wave energy converter in the following sections.

RESULTS

As was outlined in the introduction, a perfect wave termination device must create a wave of equal height but opposite phase relative to the wave that is to be terminated. This wave must only be created down–wave of the wave energy converter. For this reason, it is convenient to analyze the performance of a proposed wave energy converter in its ability to be a wave generator, before analyzing the interaction between the wave energy converter and an incoming wave. Thus the next section covers wave generation by the Cycloidal wave energy converter, followed by wave cancellation in the following section

Wave Generation

Plotted in figure 2 is a typical resulting wave pattern as a function of time. The size of the wave energy converter was cho-

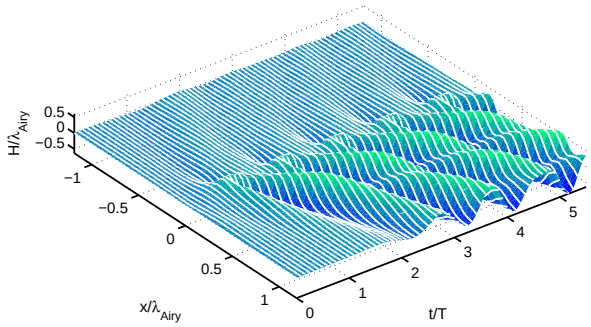

Figure 2. Wave height for wave generation using a single bladed wave energy converter. Converter size $2R/\lambda = 0.318$ located at $(y_c - R)/\lambda = 0.030$; $D/\lambda_{Airy} = 0.40$.

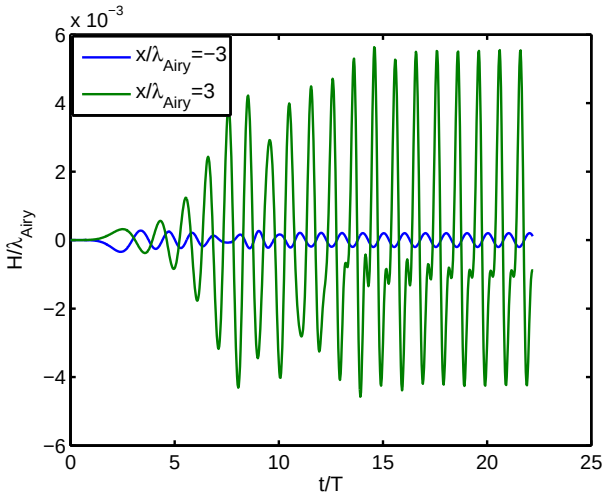

Figure 3. Wave height up–wave and down–wave of the cycloidal wave energy converter. $2R/\lambda = 0.318$ of the cycloidal wave energy converter located at $(y_c - R)/\lambda = 0.030$; $D/\lambda_{Airy} = 0.40$. All waves are evaluated at $\pm 3\lambda$.

sen to be $2R/\lambda = 0.318$, and it's submergence depth $(y_c - R)/\lambda = 0.030$. It can be seen that the dominant wave amplitudes occur on the down–wave side of the converter, while the up–wave elevations are small. A few rotations after the start of the wave energy converter at time $t/T = 0$ the flow becomes periodic in time and space. Beyond the fundamental frequency there are higher harmonic waves generated as well, as is evident in the disruption of the wave ridges traveling down–wave. More detailed analysis of

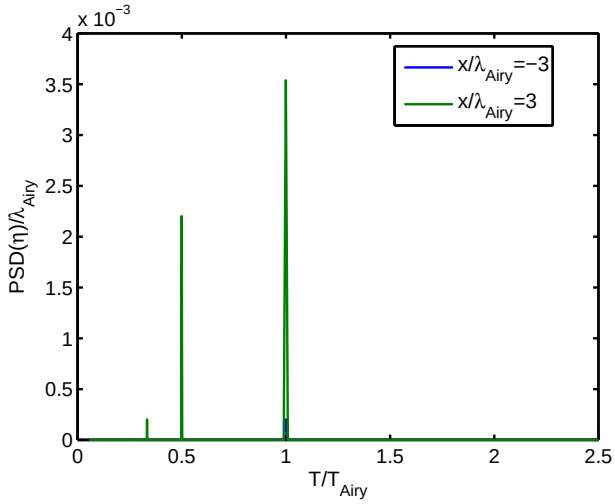

Figure 4. Power Spectral Density of the surface at $x = \pm 3\lambda$ Converter size $2R/\lambda = 0.318$ located at $(y_c - R)/\lambda = 0.030$; $D/\lambda_{Airy} = 0.40$. Data from one fundamental wave period starting at time $t/T = 30$ after the start of the Cycloidal wave energy converter is used for the analysis.

the resulting wave field at horizontal locations of $x = \pm 3\lambda$ shown in figure 3 as time signal and power spectral density in figure 4 reveals the amplitudes of the generated waves and their evolution in time. The wave pattern becomes periodic at these locations far up– and down–wave after about fifteen periods. While the amplitude of the fundamental wave of period $T_w/T_{Airy} = 1$ is the most dominant peak in the power spectral density plot in both directions, the down–wave flow field also features a peak of about half the magnitude of the fundamental wave at $T_w/T = 0.5$ as well as one at one third of the fundamental frequency. These peaks cause the disruption in the wave ridges shown in figure 2. The up–wave amplitudes caused by the wave energy converter are a very small fraction of the down–wave amplitudes. In order to evaluate the performance of the cycloidal wave energy converters, we use the wave heights of the different waves as determined by the power spectral density analysis shown in figure 4. This analysis is based on Fourier decomposition of data from a single fundamental wave period replicated 100 times in order to obtain a better frequency resolution in the decomposition.

To determine the effect of varying the Cycloidal wave energy converter radius on the resulting wave patterns, simulations were completed with constant circulation and constant submergence $(y_c - R)/\lambda_{Airy} = 0.030$. Shown in figure 5 are wave amplitudes and power down–wave and up–wave at $x = \pm 3\lambda$ for each of the first three harmonics. These were determined using power spectral density analysis as described above. The results are plotted as a function of $2R/\lambda_{Airy}$, where λ_{Airy} is the wave length of the fundamental wave. Inspecting the wave height of the fundamental wave traveling down–wave, H_1, a well defined

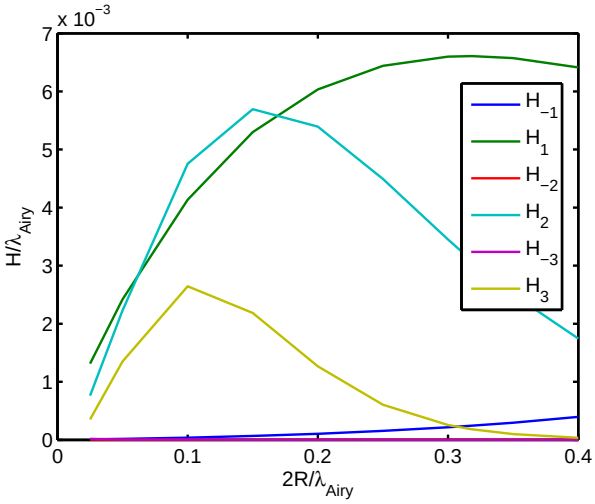

Figure 5. Wave height for different sizes $2R/\lambda$ of the cycloidal wave energy converter located at $(y_c - R)/\lambda = 0.030$. All waves are evaluated at $\pm 3\lambda$ at time $t/T = 30$ after the start of the Cycloidal wave energy converter.

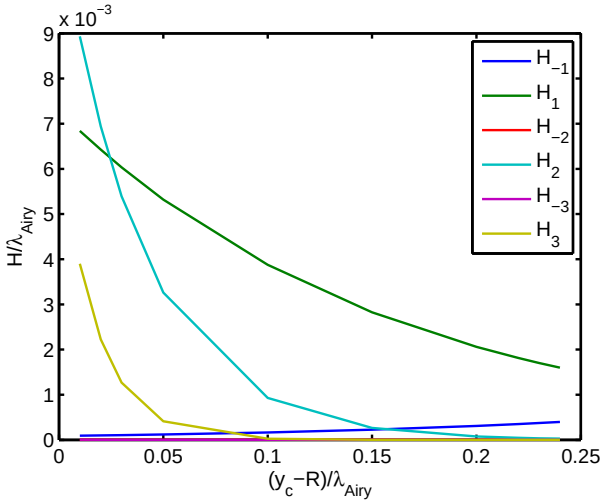

Figure 6. Wave height for different submergence depths $(y_c - R)$ of the cycloidal wave energy converter of size $2R/\lambda = 0.20$. All waves are evaluated at $\pm 3\lambda$ at time $t/T = 30$ after the start of the Cycloidal wave energy converter.

maximum can be observed at a size $2R/\lambda_{Airy} = 0.32$. However, at that size wave energy converter significant wave amplitudes are present for the second and third harmonic waves traveling down–wave. The wave height of the second and third harmonic waves reach maxima at smaller device sizes of $2R/\lambda_{Airy} = 0.15$ and $2R/\lambda_{Airy} = 0.1$, respectively. The wave height of the second harmonic even exceeds that of the fundamental wave at its peak. In the up–wave direction, the amplitude of the fundamental wave H_{-1} shows a linear increase with device size, which will be discussed later. All other harmonic waves in this direction exhibits negligible amplitudes. We would also like to point out that no significant wave amplitudes were found for any fourth and higher harmonic waves for any of the simulations conducted, which is why they are not shown.

A second parameter study where the wave energy converter size was kept constant while the submergence depth y_c/λ was varied is shown in figure 6. We present the results of this study for a device size of $2R/\lambda_{Airy} = 0.20$. The amplitude of the second harmonic down–wave traveling wave H_2 is larger than the fundamental wave height H_1 when the wave energy converter is located close to the surface. The wave heights H_1 and H_2 are equal at about $y_c - R/\lambda = 0.03$, and for larger submergence depths the wave height H_2 of the second harmonic wave drops off much faster than that of the fundamental wave. However, all waves traveling in the down–wave direction show decreasing amplitudes with increasing submergence depth, although not at the same rate. As a consequence, the power ratio improves with increasing submergence depth and asymptotically reaches a value of one. For the up–wave traveling waves, however, it can be seen that there is an almost linear increase in the amplitude of H_{-1} as the wave energy converter is moved closer to the ocean floor. This effect was not present in the deep ocean investigations reported in [4] and can thus be attributed to the interaction between the ocean floor and the cycloidal wave energy converter. However, in [4] there is a possible explanation for this effect. If the vortex strength in a deep ocean simulation is set to zero for the bottom portion of the vortex travel, an increase in amplitude of the wave H_{-1} was found in [4]. The increase in amplitude of H_{-1} shown in figure 6 as the wave energy converter approaches the ocean floor is very similar to that. Thus a possible explanation for the increase in H_{-1} lies in a reduced effectiveness of the vortex in canceling the up–wave fundamental wave during its bottom half travel while it is close to the ocean floor.

As shown in figure 6, for a single wave energy converter the presence of a harmonic wave of twice the fundamental frequency is a dominant effect when the wave energy converter is placed close to the water surface, which otherwise would be a favorable location since the amplitude of the fundamental wave is maximized there. By adding a second hydrofoil to the wave energy converter, located opposite to the first one and having equal circulation but of opposite sign, the generation of the harmonic wave can be entirely prevented. This is shown in figure 7, where the wave created by the first and second vortices are shown, along with the superposition of both vortices. While the fundamental wave amplitudes from both waves can be seen to add to create a larger amplitude fundamental wave, the first harmonic components of both waves entirely cancel out. This is very much desired as it prevents the harmonic wave generation which is detrimental to the performance of the device.

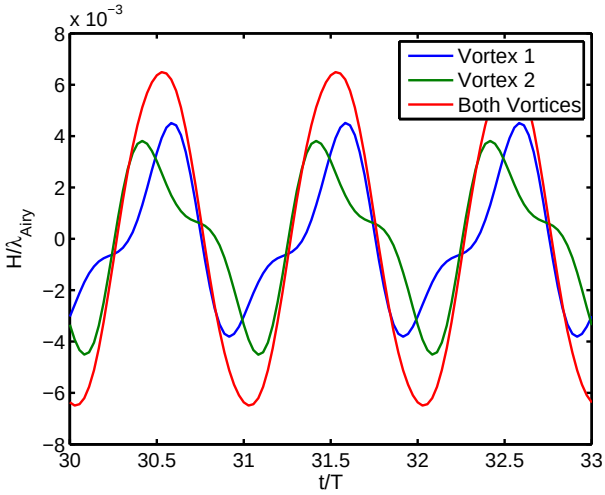

Figure 7. Superposition of waves from two vortices located 180° apart with non dimensional circulation $\Gamma/(CR) = [-0.035, 0.035]$. The cycloidal wave energy converter of size $2R/\lambda = 0.318$is located at $(y_c - R)/\lambda = 0.03$. All waves are evaluated at $x = 3\lambda$

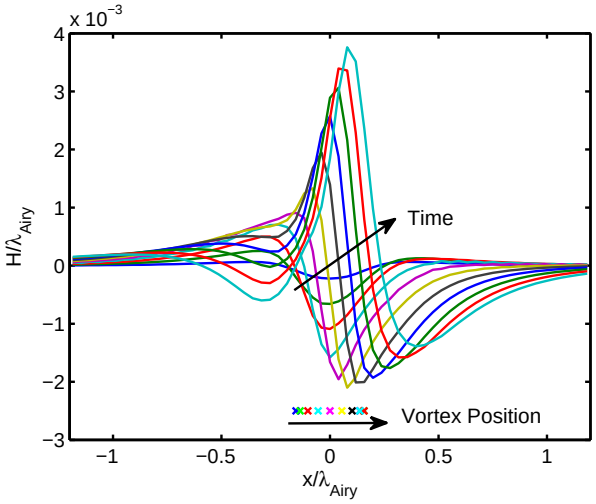

Figure 8. Water surface as the second vortex approaches and moves underneath the free water surface during the first rotational cycle. $2R/\lambda_{Airy} = 0.318$; $(y_c - R)/\lambda_{Airy} = 0.03$. The two vortices are spaced 180° apart with non dimensional circulation $\Gamma/(CR) = [-0.035, 0.035]$. Shown are the instantaneous surface elevations as well as the horizontal location of the vortex

Insight into the physical mechanism by which the rotating hydrofoils are creating the observed wave pattern can be gained by inspection of the local water surface displacement caused by the hydrofoils or vortices. The first inspection of figure 8 reveals that vortex two, which has negative circulation, causes a depression of the water surface as it approaches from below. This observation is consistent with the high and low pressure that a corresponding hydrofoil would create on its pressure and suction side. On closer inspection, the depression caused by vortex two travels along with the vortex in the same direction and at approximately the same velocity. This observation is a hint at a possibly important parameter, which is the ratio between the velocity at which the hydrofoil travels on its circular path, U_{rot}, and the wave travel velocity or celerity C. The vortex travel velocity $U_{rot} = R\,\omega_c$ only depends on the device size $2R/\lambda_{Airy}$ for a constant rotational velocity ω_c of the wave energy converter, while the celerity C of the fundamental wave is constant. For a device size $2R\lambda_{Airy} = 0.3$ the velocity ratio U_{rot}/C_{Airy} is close to unity indicating a match between hydrofoil rotation velocity and wave travel velocity. As $2R/\lambda_{Airy} = 0.32$ is the device size for which the fundamental wave height is maximized (see figure 5), it appears that the fundamental wave amplitude is maximized if the velocity of the hydrofoil matches that of the wave. Further evidence that this is true can be gained by inspecting the harmonic wave amplitudes in figure 5. Not just is the amplitude of the fundamental wave height H_1 maximized at the same device size, but the peak amplitudes of the harmonic waves that travel at half (for W_2) and one third (for W_3) of the celerity of the fundamental wave occur at exactly one half or one third of the device size, which is $2R/\lambda_{Airy} = 0.15$ and $2R/\lambda_{Airy} = 0.1$ respectively.

Thus, the generation of all harmonic waves is maximized once the hydrofoil travel velocity matches the respective wave celerity. Based on these observations we conclude that for optimal wave generation two design conditions have to be met:

$$\begin{aligned} \omega_c R &= C_{Airy} \\ \omega_c &= \omega_{Airy}. \end{aligned} \tag{10}$$

This result makes also physical sense as Airy wave theory assigns a distinct wave celerity to each wave of a given period, and thus waves with a mismatch between their period T and the celerity C induced by the vortex velocity can not be sustained.

Postulating a match of hydrofoil velocity and wave celerity as expressed in equation 10, we obtain with the airy wave equation 5 the following optimal device size:

$$\frac{2R}{\lambda_{Airy}} = \frac{1}{\pi} \approx 0.318. \tag{11}$$

This result is independent of the type of wave, that is it holds for shallow, intermediate and deep water waves. In [4] it is shown that the interaction of the cycloidal wave energy converter with deep ocean waves shows the exact same optimal device size, both for single vortex as well as flat panel simulations.

Wave Cancellation

With the two–hydrofoil cycloidal wave energy converter characterized in the previous section, it is interesting to attempt cancellation of an incoming Airy wave. Figure 9 shows the water surface elevation as a function of time where the cycloidal wave energy converter is interacting with an incoming Airy wave. This requires feedback of the incoming wave amplitude and phase to the motion of the cycloidal wave energy converter. We employ the following linear feedback laws:

$$\begin{aligned} \delta(t) &= \omega t + \theta \\ \Gamma &= k_\Gamma H_{Airy}. \end{aligned} \tag{12}$$

where $\delta(t)$ is the angle of the cycloidal wave energy converter main shaft, and θ is a constant phase shift between the wave motion and the converter rotational angle. The fixed feedback gain k_Γ is adjusted such that the amplitude of the wave H_1 created by the wave energy converter matches that of the incoming Airy wave exactly. Figure 10 demonstrates the impact of the phase between the incoming wave and the rotation of the cycloidal propeller on the wave height. While there is very little impact of the feedback phase on all waves other than the fundamental wave down–wave of the converter, the down–wave amplitude shows a linear relationship for feedback phases above and below the optimal phase angle $\theta = 10^\circ$. The resulting down–wave wave pattern as a function of time is shown in figure 9 for the optimal feedback phase of $\theta = 10^\circ$. For this phase, the fundamental down-wave amplitude is close to zero, while there are still higher harmonic waves present, most prominently the third harmonic. In this inviscid simulation, more than 95% of the incoming wave energy is converted to shaft power, while the remainder is lost to harmonic waves as seen in the wave height plot. The same simulation result is also shown in figure 11 where the temporal evolution of the wave cancellation can be seen. For the cancellation to be effective in the spatial domain shown, about 5 wave periods are necessary. While the present simulation does not model losses due to viscous skin friction and pressure drag of a typical hydrofoil, we estimate these to be less than 30% of the incoming wave power for a typical hydrofoil based on published lift to drag ratios for symmetric (NACA 0015) hydrofoils operating in typical ocean waves, for further details see [4].

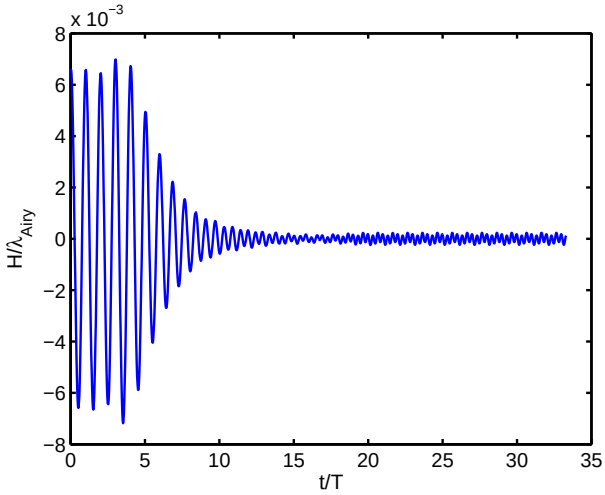

Figure 9. Wave height for a feedback phase of $\theta = 10^\circ$ of the cycloidal wave energy converter with two vortices spaced 180° apart with non dimensional circulation $\Gamma/(CR) = [-0.035, 0.035]$.

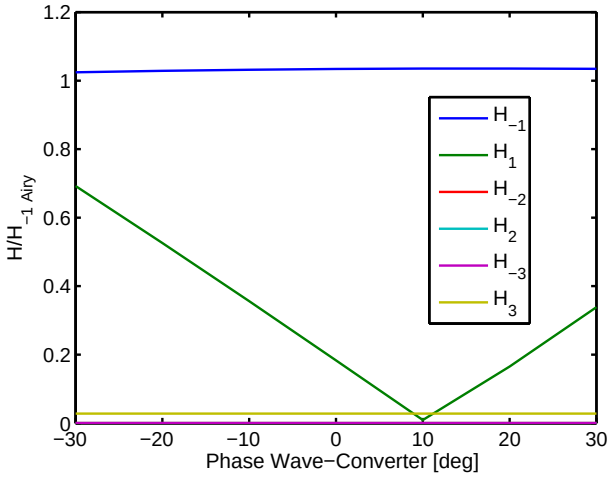

Figure 10. Wave heights vs wave phase of the cycloidal wave energy converter with two vortices spaced 180° apart with non dimensional circulation $\Gamma/(CR) = [-0.035, 0.035]$. All waves are evaluated at $\pm 3\lambda$ at time $t/T = 30$ after the start of the Cycloidal wave energy converter. Shown are harmonic amplitudes.

DISCUSSION AND SUMMARY

We show that the well known cycloidal propeller can be used both as an efficient wave maker, as well as a wave termination device for intermediate ocean waves. We show inviscid two-dimensional simulation results for cycloidal wave energy converters featuring both a single blade as well as two blades spaced 180° apart. In these simulations, the blades of the wave energy converter are modeled as a point vortex. For wave generation, we find that it is possible to create a single Airy type wave that only travels in one direction, with no wave being generated in the other direction. The direction of travel is controlled by the rotation direction. Depending on geometry choices for converter radius and submergence depth, in addition to the fundamental wave traveling in one direction up to two higher harmonic waves

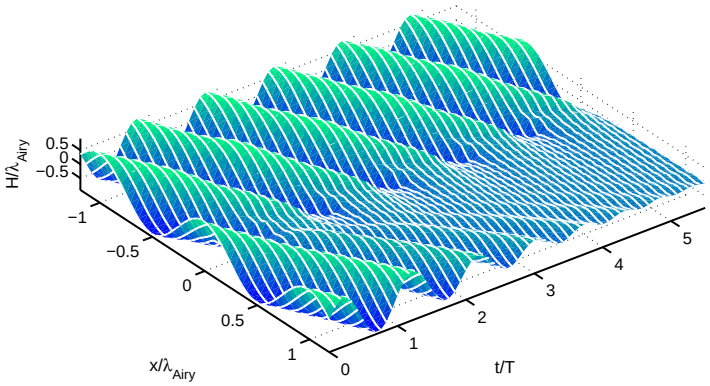

Figure 11. Water surface—time plot for wave cancellation of an Airy wave travelling in the positive x direction using a cycloidal wave energy converter with two hydrofoils. The converter is located at $x/\lambda_{Airy} = 0$, rotation is started at $t/T = 0$

traveling up – and down–wave can be observed. A parameter study investigating the impact of wave energy converter size shows that the largest amplitude fundamental wave is obtained for a device of size $2R/\lambda_{Airy} = 1/\pi$. This size corresponds to an exact match between the rotational velocity of the hydrofoil and the wave velocity. As the cycloidal wave energy converter is moved closer to the ocean floor, a increase in the amplitude of the fundamental wave traveling up–wave is seen, which is a marked difference from deep water results that do not show this effect.The single sided wave generated by the cycloidal wave energy converter is perfectly suited to extract energy from an incoming plane Airy wave. In order to achieve this, the motion of the wave energy converter needs to be synchronized in frequency and phase locked to the incoming wave using feedback control, and the circulation of the converter's hydrofoils needs to be adjusted to produce a wave of matching amplitude. If this is accomplished, in the two dimensional inviscid limit, more than 95% of the incoming wave energy can be extracted from the wave achieving wave termination. It should be pointed out that as the water depth approaches that of a shallow water wave, the efficiency of this wave energy converter will be reduced since the device size $2R$ cannot exceed the water depth D, and thus the optimal velocity match as described above cannot be achieved. In this case it may be more advantageous to orient the cycloidal wave energy converter with its shaft aligned with the vertical direction, as described for example in [9]. We intend to explore this and other possible means for a cycloidal wave energy converter to interact efficiently with shallow water waves in future research.

ACKNOWLEDGMENT

We would like to acknowledge the fruitful discussions with our colleagues at the Air Force Academy, most importantly Drs. Seidel and Jirasek as well as Mr. Fagley, as well as computational support from the Air Force Academy Modeling and Simulation Center led by Dr. Bergeron. This material is based upon activities supported by the National Science Foundation under Agreement No ECCS-0801614. Any opinions, findings, and conclusions or recommendations expressed are those of the authors and do not necessarily reflect the views of the National Science Foundation.

REFERENCES

[1] Boyle, G., 2004. *Renewable Energy - Power for a sustainable future*. Oxford University Press.

[2] Bedart, R., 2005. Final summary report - offshore wave power feasibility demonstration project. Tech. rep., E2I EPRI Global, WP 009 - US Rev 1.

[3] Falnes, J., 2002. *Ocean Waves and Oscillating Systems*. Cambridge University Press.

[4] Siegel, S. G., Jeans, T., and McLaughlin, T., 2009. "Deep ocean wave energy conversion using a cycloidal turbine". *J. Fluid Mech.,* ***submitted***.

[5] Wehausen, J., and Laitone, E., 1960. *Surface Waves, Handbook of Physics, Vol.9*. Springer-Verlag.

[6] Hermans, A. J., and van Sabben, E., 1990. "A device to extract energy from water waves". *Applied Ocean Research Computational Mechanics Publications,* ***Vol. 12, No. 4***, p. 5.

[7] Newman, J. N., 1977. *Marine Hydrodynamics*. MIT Press.

[8] Pinkster, J., and A.J.Hermans, 2007. "A rotating wing for the generation of energy from waves". In 22nd IWWWFB Conference, Plitvice, Croatia.

[9] Siegel, S. G., 2006. "Cyclical wave energy converter". *pending U. S. and pending / awarded International Patent applications*.